CHANGES IN ATOMIC STRUCTURE OF AMORPHOUS IRON(III) SULFATE AS A FUNCTION OF HYDRATION: IMPLICATIONS FOR MARTIAN SOILS AND SAMPLE RETURN. J. C. Gregerson[1], A. D. Rogers[1], L. Ehm[1,2], and J. B. Parise[1,2], [1]Stony Brook University, Stony Brook, NY, 11794-2100, jason.gregerson@stonybrook.edu. [2]Brookhaven National Lab, Upton, NY 11973-5000.

Introduction: The CheMin instrument on MSL has measured 20-50 wt% amorphous component in soils and 15-45 wt% amorphous component in rocks in Gale crater [1-5]. This amorphous component is enriched in both iron and sulfur and contains water [1,3,6,7], suggesting amorphous iron sulfate as a possible component of the amorphous fraction [3,7].

Previous lab studies have shown that amorphous sulfates can form via rapid dehydration of aqueous solutions [8-12]. Amorphous ferric sulfates are sensitive to changes in temperature and relative humidity (RH) and will hydrate and dehydrate in response [10]. Additionally, the rate of dehydration controls the hydration state of the amorphous solid [10-12].

In crystalline ferric sulfates of varying hydration state, the amount of hydration dictates the enthalpy of formation and entropy of the phases [13], which in turn relate to the stability of the structure upon changes in temperature and pressure. Crystalline ferric sulfates also have different atomic structures depending on hydration state. The atomic structure of a crystalline or amorphous phase can be assessed via X-ray Pair Distribution Function (PDF) analysis.Though the atomic structure of a limited set of amorphous ferric sulfates has been previously reported [11], the effect of varying hydration state on the atomic structure of amorphous ferric sulfates is unknown.

This study seeks to explore the variations in short-range structure of amorphous ferric sulfates as a function of hydration state. This information could provide insight into the expected changes in hydration and crystallinity that these phases might undergo on the Martian surface and subsurface but also during sample caching and return.

Materials and Methods: Anhydrous $Fe_2(SO_4)_3$ (99.998% purity) was deliquesced in a 99% RH environment buffered by deionized water to form a solution with a concentration of 32.3wt% $Fe_2(SO_4)_3$.

This solution was divided into seven aliquots and dehydrated using a variety of dehydration methods to produce a suite of amorphous ferric sulfates with varying hydration states (**Table 1**). These methods include vacuum-induced boiling, dehydration at 11% RH, and heating to 60°C. Additionally, two samples were dehydrated, deliquesced, and dehydrated again. Samples were weighed after each step to measure changes in water content.

Table 1. Dehydration pathways from ferric sulfate solution and compositions of amorphous samples produced.

Dehydration Pathway	Final Hydration State
Vacuum → Deliquescence → Vacuum (Cycled)	$Fe_2(SO_4)_3$*4.01 H_2O
Vacuum	$Fe_2(SO_4)_3$*4.68 H_2O
Low RH → Vacuum	$Fe_2(SO_4)_3$*5.18 H_2O
Vacuum → Low RH	$Fe_2(SO_4)_3$*6.13 H_2O
Low RH at 60°C	$Fe_2(SO_4)_3$*7.56 H_2O
Low RH	$Fe_2(SO_4)_3$*8.33 H_2O
Low RH → Deliquescence → Low RH (Cycled)	$Fe_2(SO_4)_3$*8.46 H_2O

Amorphous samples were examined using total X-ray scattering at beamline 28-ID-1 at National Synchrotron Light Source – II, Brookhaven National Laboratory. This data was input into the software xPDFsuite to generate a Pair Distribution Function (PDF) for each sample.

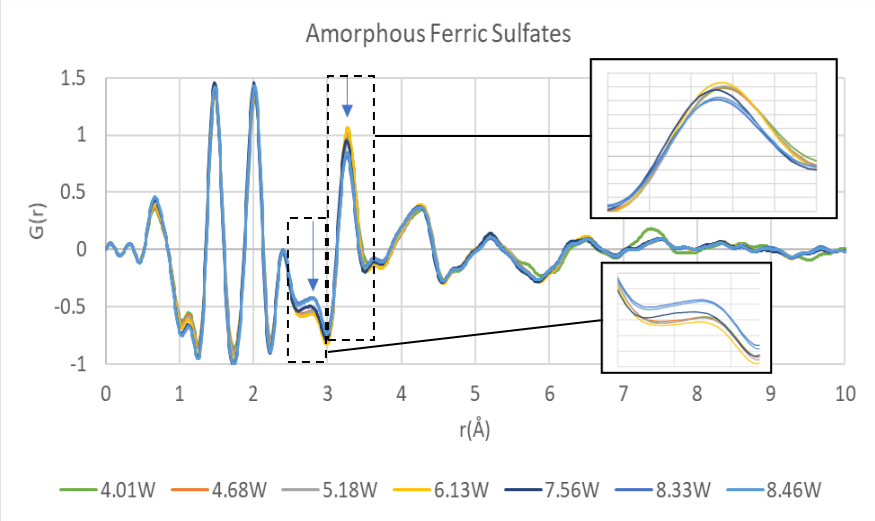

Figure 1. PDF comparison of this work's amorphous ferric sulfate samples. Each sample is labeled by hydration state that can be referred to in Table 1.

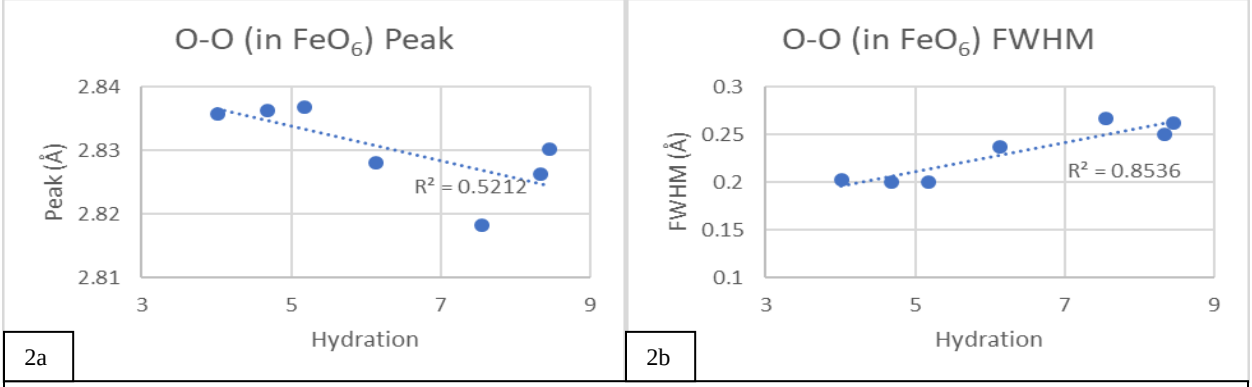

Figures 2a-2d. Scatter plots showing each amorphous ferric sulfate sample as a point. These plots show peak position (2a and 2c) and full-width-half-maximum (FWHM) (2b and 2d) vs amount of stoichiometric waters (hydration). 2a and 2b show this information for the FeO_6 O-O peak. 2c and 2d show this information for the Fe-S peak. Linear fits are shown for all plots with R^2 values.

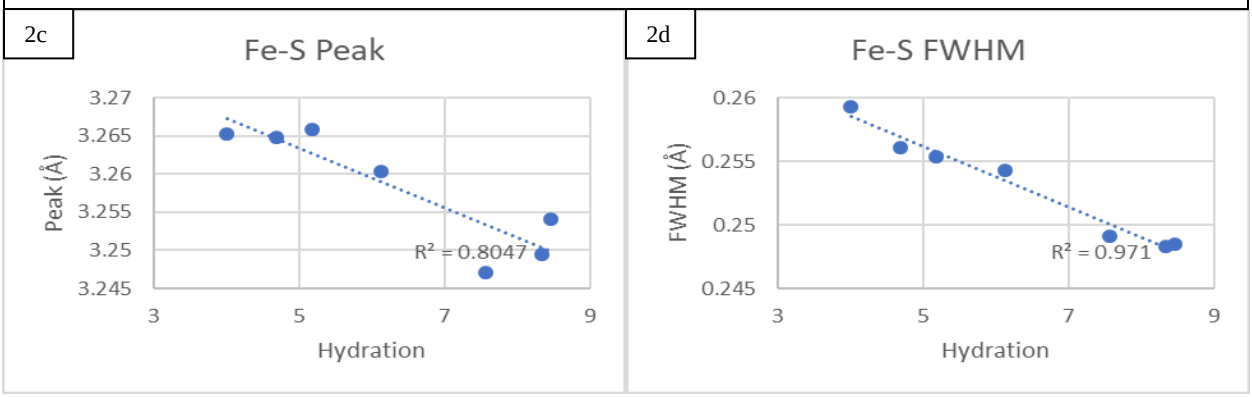

Results: The PDFs of each sample are shown in **Figure 1**. Peaks representing short-range (<4.5 Å) interatomic distances can be fit by comparing the distances in these amorphous samples to those in mikasaite, a crystalline ferric sulfate [14].

Differences in PDF peaks among amorphous samples with different hydration can be seen in two peaks: the peaks corresponding to the O-O distances in FeO_6 octahedra (~2.75 Å) and the Fe-S distance with a corner-shared O (~3.3 Å) (**Figure 1**).

The peak positions correspond to the average distance between atoms, and the peak broadness (represented as full-width-half-maximum, FWHM) corresponds to the range of distances between atoms. For the FeO_6 O-O distance, the average distance decreases with increasing hydration (**Figure 2a**) and the range of distances increases (**Figure 2b**). For the Fe-S distance, the average distance decreases with increasing hydration (**Figure 2c**) and the range of distances decreases (**Figure 2d**).

Discussion: The structural trends identified in this work provide information on the effects of hydration and dehydration of a potential component of Martian soils. These trends could prove important in understanding how soil samples could change during sample caching and return, in response to temperature changes in a sealed environment. The data provided in this work may also assist in back-modeling the hydration state and crystallinity of what phases were initially present during sample caching from a study of what materials are present upon return.

Acknowledgements: This work was supported by the NASA SSW and PME awards 80NSSC18K0535 and 80NSSC18K0516.

References: [1] Bish, D. L. et al. (2013) Science, 341. [2] Blake et al. (2013), Science, 341. [3] Dehouck et. al. (2014), J. Geophys. Res. Planets, 119, 2640–2657. [4] Vaniman et al. (2014), Science, 343. [5] Achilles et al. (2017), J Geophys. Res. Planets, 122 [6] Leshin et al. (2013), Science, 341. [7] McAdam et al. (2014), J. Geophys. Res. Planets, 119. [8] Xu, W. Q. et al. (2009) Am. Mineral., 94, 1629–1637. [9] Xu, W. Q. and Parise, J. B. (2012), Am. Mineral., 97, 378–383. [10] Wang et al. (2012), Icarus, 218, 1629-1637. [11] Sklute, E. C. et al. (2015) JGR, 120, 809- 830. [12] Sklute E. C. et al. (2018) Icarus, 302, 285-295. [13] Hemingway, B. et al. (2002) U.S. Geological Survey Open File Report 02-16113 [14] Christidis and Rentzeperis (1976) Zeitschrift für Kristallographie, 114, 341-352.